Research Paper

A novel circular RNA DNAH1 inhibits osteosarcoma progression by interacting with miR-663a

Peifeng Li[1], Ying Zhang[1], Shimin Mu[1], Jitian Li[1]

[1]Department of Hip Injury, Henan Luoyang Orthopedic Hospital, Henan Provincial Orthopedic Hospital, Henan Institute of Orthopedic and Traumatology, Luoyang, Henan, China

Correspondence to: Jitian Li; **email:** jitianlee@hotmail.com
Keywords: circ-DNAH1, miR-663a, MAPK/ERK signaling pathways, osteosarcoma
Received: March 19, 2021 **Accepted:** September 18, 2021 **Published:**

ABSTRACT

Osteosarcoma (OS) is a bone malignancy mostly found in adolescents accounting for about 60% of malignant bone tumors. Despite the availability of limb-saving surgery, multiagent and dose-intensive chemotherapy, the survival rate is low for patients with axial OS and distant metastasis. Moreover, the etiology of OS has not been fully understood, greatly impeding the development of new treatments. Recently, circular RNAs (circRNAs) emerge as a new class of noncoding RNAs and are implicated in oncogenesis as a sponge for microRNAs. Here, we report the identification of circ-DNAH1, a novel cytoplasmic circRNA that is generated from exon 67 to 70 of *DNAH1* (Dynein Axonemal Heavy Chain 1) and inhibits the OS progression. Circ-DNAH1 is downregulated in OS, and the lower levels of circ-DNAH1 are inversely correlated with survival rates. Functionally, overexpression of circ-DNAH1 inhibits the proliferation, migration and invasion of OS cells *in vitro*. Mechanistically, circ-DNAH1 sponges miR-663a, a microRNA that functions as an oncogene and promotes OS progression through EMP3 and MAPK/ERK signaling pathways. Moreover, overexpression of circ-DNAH1 reverses miR-663a-induced enhancement of cell proliferation, migration and invasion of OS cells. Furthermore, enforced expression of circ-DNAH1 suppresses OS growth and metastasis *in vivo*. Together, we have characterized a novel circular RNA, circ-DNAH1 that acts as a tumor suppressor in OS development and serves as an independent prognostic factor for OS patients.

INTRODUCTION

Osteosarcoma (OS) is one of the most common primary bone cancers with the highest prevalence in adolescence [1, 2]. OS is formed by the transformed cells originated from mesenchyme that is partially osteoblastic differentiated and produces malignant osteoid [3]. OS mostly occurs in the long bones including lower limbs, and more than half of OSs were found around the knee. Other than that, 10-15% of OSs develop in the axial skeleton, such as the pelvis [4, 5].

The distant metastasis rate of OS is high with 40% of OS patients having a local or distant recurrence, and the majority of relapses exhibiting lung metastases [6]. Complete surgical resection followed by multiagent, dose-intensive chemotherapy is the mainstay of OS treatment, which has significantly improved the 5-year event-free survival to 60-70% for the non-metastatic OSs that are restricted to the extremity of long bones [3]. However, the prognosis is significantly poorer in patients with axial OS and distant metastasis with survival rates lower than 20% [7].

The molecular pathogenic mechanisms of OS have not been well understood. Aberrations in several pathways including p53, RBI, DLG2 and PI3K/mTOR have been reported to be relevant [8, 9]. In addition to genetic mutations, microRNAs (miRNAs) also modulate OS development. For example, miR-214 is upregulated in OS and likely functions as an oncogene; however, the expressions of miR-382, miR-134 and miR-544 are

inversely correlated with OS development, implying that the three microRNAs function as tumor suppressors [10, 11].

Circular RNAs (circRNAs), one type of non-coding RNAs (ncRNAs), play important roles in regulating gene expression [12, 13]. CircRNAs are generated from genomic DNA by back splicing or from lariat structures via exon skipping. Without poly(A) tails, circRNAs are more stable than mRNAs. CircRNAs are functionally versatile, regulating mRNA translation, gene transcription and splicing by sponging microRNAs or decoying proteins in protein-RNA complexes. For example, CDR1as, a circRNA derived from cerebellar degeneration-related protein 1 (CDR1), contains multiple binding sites for miR-7, a mammalian miRNA [14].

Many circRNAs are dysregulated in cancer cells, thereby regulating the activities of important pathways for tumor development, such as apoptosis, angiogenesis and cell cycle progression [15]. For example, CDR1as has been found to act as a broad tumor suppressor [16]. Three circRNAs, circUBAP2, circ-0016347 and CDR1as were reported to be upregulated in OS and promote OS progression through sponging miR-143, miR-214 and miR-7, respectively [17–19]. Recently, one study using circRNA microarray reveals the differentially expressed circRNAs between human OS cell lines and human osteoblasts, laying the foundation for further studies of circRNAs involved in OS progression [20]. Through analysis of the expression data deposited in the NCBI's Gene Expression Omnibus (GEO) database, we found that a novel cytoplasmic circRNA, circ-DNAH1 that is derived from exon 67 to 70 of *DNAH1* (Dynein Axonemal Heavy Chain 1), was significantly downregulated in OS. Next, we further characterized the role of circ-DNAH1 in OS development and probed its potential as a prognostic marker.

MATERIALS AND METHODS

Clinical patient samples

Sixty pairs of OS and adjacent (distance, ≥3 cm) para-carcinoma tissue samples were collected from Luoyang Orthopedic-Traumatological Hospital (Luoyang, China). A total of 60 patients were enrolled from January 2008 to January 2018. The OS patients were diagnosed by two pathologists and had not received any therapy before sample collection. The dissected tissues were instantly frozen in liquid nitrogen and stored at -80° C for further use. The protocols for sample collection and experiments were approved by the ethics committee of the Luoyang Orthopedic-Traumatological Hospital and performed in accordance with the guidelines of the Declaration of Helsinki. Written informed consent was reviewed and signed by all patients.

Chemicals and reagents

All chemicals, unless stated otherwise, were obtained from Sigma-Aldrich (St Louis, USA). The cell culture reagents were bought from Hyclone (Logan, UT, USA). The services of primer synthesis and construct sequencing were provided by Shanghai Genechem Co. (Shanghai, China). The virus for transfection was obtained from Shanghai Genechem Co.

Cell culture and transfection

Five human OS cell lines, i.e., HOS, 143B, Saos2, MG63 and U2OS, were grown in Dulbecco's modified Eagle's medium (DMEM) containing 10% fetal bovine serum (FBS) and 4.5 g/L glucose at 37° C with 5% CO_2. MG63 and U2OS cells were transfected at 50% confluence using Lipofectamine 3000 (Invitrogen, Grand Island, NY, USA).

Quantitative real-time PCR (qPCR)

Total RNAs were isolated using the Trizol reagent (Invitrogen, Grand Island, NY, USA). Real-time qPCRs for quantifying human DNAH1, circ-DNAH1 and miR-663a were performed on StepOnePlus Real-time PCR system (Applied Biosystems, Waltham, MA, USA) using SYBR Green PCR Master Mix (Transgen, Beijing, China). Relative expression levels of targets were calculated by $2^{-\Delta\Delta Ct}$ method. GAPDH (glyceraldehyde 3-phosphate dehydrogenase) or U6 small nuclear RNA were used as the internal control. All the primers were listed in Supplementary Table 1.

Western blot

Total cellular lysates (8 μg protein per sample) were separated on a 10-12% of SDS- PAGE gel and subsequently transblotted to the polyvinylidene fluoride membrane (Merck Millipore, Darmstadt, Germany). Following blocking in 10% non-fat milk, the membranes were treated with the primary antibodies followed by the treatment with peroxidase-conjugated secondary antibodies. The protein bands were visualized with Clarify Western ECL Substrate (Bio-Rad, Hercules, CA, USA). Finally, the band densities were measured by the Image J software (NIH, Bethesda, MD, USA). The primary antibodies used in this study included: EMP3 (ab236671, Abcam, 1:1000 dilution), p-c-RAF (ab225628, Abcam, 1:500 dilution), MEK (ab32091, Abcam, 1:1000 dilution), phospho-MEK (ab278564, Abcam, 1:1000 dilution), ERK (ab184699, Abcam, 1:1000 dilution), phospho-ERK (ab223500,

Abcam, 1:1000 dilution) and GAPDH (ab8245, Abcam, 1:1000 dilution). The secondary antibodies used in this study were: anti-mouse IgG H&L (ab150113, Abcam, 1:10000 dilution) and anti-rabbit IgG H&L (ab150077, Abcam, 1:10000 dilution).

Fluorescence *in situ* hybridization (FISH)

The Fluorescent probe for detecting circ-DNAH1 was designed and synthesized by Genepharma (Shanghai, China). The florescent signal was developed and detected by a Fluorescent *In Situ* Hybridization Kit (Genepharma, Shanghai, China). Briefly, the probe against circ-DNAH1 (5' Cy3- AAAGCTTCCGAGCT ATCCACC 3') was synthesized, end-labeled with 6-carboxyfluorescein (FAM), and purified by high-performance liquid chromatography (HPLC). MG63 and U2OS cells were fixed in 500 μL 10% formalin for 30 min at 25° C. Then, the coverslips were washed three times (5 min/time) in phosphate buffered saline (PBS). Next, the cells were dehydrated in ethanol series (50, 80 and 95%) before hybridization. Subsequently, the FAM-labeled probe was diluted in 500 μL of hybridization buffer (0.7 M NaCl, 0.1 M Tris, 0.1% sodium dodecyl sulfate, 10 mM EDTA, pH 8.0) and was applied to the cells for hybridization for 15 min at 55° C. After that, the samples were rinsed with the preheated probe-free hybridization buffer (60° C) for 5 min. Then, the cells were counterstained for 10 min in the dark with 30 μL of mounting medium containing 4',6-diamidino-2-phenylindole (DAPI) (dilution 1:1000). Finally, the images were taken on a fluorescence microscope (Leica Microsystems, Meinheim, Germany).

Pull-down assay with biotinylated circ-DNAH1 probe

A biotinylated probe against the junction area of circ-DNAH1 was designed and synthesized by Tsingke (Wuhan, China), and a probe against a random sequence was used as a negative control. The probes were then fully mixed by vortex and incubated with streptavidin magnetic beads (Life Technologies, USA) at room temperature for 2 h to generate probe-coated beads. A total of 1×10^7 MG63 or U2OS cells were lysed, and the cell lysates were incubated with probe-coated beads at 4° C overnight. The beads were washed and the miRNAs were extracted using Trizol and quantified by qRT-PCR.

Pull-down assay with biotinylated miR-663a

MG63 and U2OS cells transfected with 50 nM of biotinylated miR-663a mimics or nonsense control (Tsingke, Wuhan, China) were harvested 24 h after transfection and lysed. The cell lysates were then incubated with streptavidin magnetic beads (Life Technologies) for 3 h. Finally, the RNAs bound to biotinylated miR-663a were isolated using Trizol, and the levels of circ-DNAH1 were determined by qRT-PCR.

Luciferase reporter assay

The luciferase reporter constructs, pGL3-Firefly-Renilla containing circ-DNAH1-WT and circ-DNAH1-MUT sequence were synthesized by Gene Pharma Co. (Shanghai, China). The firefly luciferase reporter plasmids (pGL3) and renilla luciferase plasmids (pRL) were construed by YEASEN Co. (Shanghai, China). The luciferase reporter plasmids were co-transfected into cells with miR-663a mimics, miR-NC and pRL using Lipofectamine™ 2000 reagent (Invitrogen, USA). After 36 h, the firefly luciferase and renilla luciferase activities were measured. The effects of miR-663a mimics on the luciferase reporter were calculated based on the ratio of firefly luciferase/Renilla luciferase activity.

Cell counting Kit-8 (CCK-8) assay

The proliferation of MG63 and U2OS cells was determined by the Cell Counting Kit-8 (CCK-8, Dojindo, Japan) according to the manufacturer's instructions. Briefly, 5×10^3 MG63 or U2OS cells were seeded into each well of a 96-well plate. After incubation for 72 h, CCK-8 solution (10 μL/well, Dojindo, Japan) was applied to each well. After incubation for another 2 h, CCK-8 optical density (OD) values at 450 nm were measured.

Transwell migration and invasion assays

To examine cell migration, MG63 or U2OS cells (1×10^5 cells in 300 μL serum-free medium) were seeded into a Transwell top chamber with a pore of 8 μm in size (Millipore). DMEM containing 10% FBS was added to the bottom chambers and incubated with the cells for 24 hr. Then, the non-migrated cells on the upper surface were discarded. The migrated cells on the lower surface were fixed with ice-cold 4% paraformaldehyde and stained with crystal purple (Dingguo, Beijing, China). For quantitation, the membranes were incubated with 50% acetic acid and the absorbance was measured with the Microplate Reader (Biotek, Beijing, China).

To measure cell invasion, MG63 or U2OS cells were seeded into a Transwell top chamber (Millipore) coated with 10 μm-thick Matrigel (BD). DMEM containing 10% FBS was added to the bottom chambers and incubated for 24 hr. Subsequently, the cells migrating through the Matrigel were fixed,

stained with crystal purple and quantified as described above.

Scratch assay

MG63 and U2OS cells were cultured in a 6-well plate to 100% confluence within 24 hours. A 200 μL pipet tip was moved straightly against the cell monolayer to create a scratch. Then, the cell debris was removed, the culture medium in each well was replaced and the cells in plates were incubated in a CO_2 incubator. At 0, 24, 48 h post incubation, the scratch was examined under an inverted phase-contrast microscope. The images acquired for each sample were analyzed and quantified using Image Pro-Plus software (Media Cybernetics). Finally, the photographed regions were aligned, and the width of each scratch was calculated.

circ-DNAH1 shRNA

Two shRNAs targeting non-overlapping sequences (shRNA-1/2) of circ-DNAH1 were sub-cloned into GV248 (hU6-MCS-Ubiquitin-EGFP-IRES-puromycin) constructs (Shanghai Genechem Co.). Then, the constructs were transfected into HEK-293 cells with lentivirus package plasmid mix (Shanghai Genechem Co.). The generated circ-DNAH1 shRNA lentivirus, LV-circ-DNAH1 shRNA-1/2 were added toMG63 and U2OS cells cultured in polybrene medium). Stable cells were selected by puromycin (5.0 μg/mL, for 4-5 passages). Silencing of circ-DNAH1 in stable cells was confirmed by qPCR. MG63 and U2OS cells transfected with a lentiviral scramble shRNA were used as a negative control.

Ectopic overexpression of circ-DNAH1 and miR-663a

The full-length of circ-DNAH1 and pri-miR-663a were synthesized and sub-cloned in a lentiviral GV248 construct (Shanghai Genechem Co.). The constructs were co-transfected with lentivirus package plasmid mix into HEK-293 cells to generate circ-DNAH1-expressing lentivirus (LV-circ-DNAH1) and miR-663a-expressing lentivirus (LV-miR-663a). Following filtration and enrichment, LV-circ-DNAH1 or LV-miR-663a was added to MG63 and U2OS cells. Puromycin was used to select stable cells. MG63 and U2OS infected with lentivirus with empty vector were used a negative control.

miR-663a inhibition

The miR-663a inhibitor precursor (Shanghai Genechem) was subcloned into the GV248 vector and co-transfected into 293 T cells with lentivirus package plasmids to generate mtagomiR-663a lentivirus (LV-antagomiR-663a). The LV-antagomiR-663a was transduced to MG63 and U2OS cells for 24 h. Puromycin was added to select the stable cells. miR-663a inhibition in the stable cells was confirmed by qPCR.

RNA immunoprecipitation (RIP)

MG63 and U2OS cells were lysed in a complete RIP lysis buffer (Beyotime Biotechnology, Suzhou, China), and the cell lysates (800 μg lysates per sample) were incubated with the magnetic beads conjugated with anti-Argonaute 2 (07-590, Sigma) or control anti-IgG antibody (I4506, Sigma) for 12 h. The beads were washed and incubated with Proteinase K to remove the unbound proteins. The recovered RNA was subjected to qPCR analysis, and the results were normalized to the input control.

OS xenograft transplant model

MG63 and U2OS cells (5×10^6) were subcutaneously injected into the breast fat pads of 4-week-old female BALB/c nude mice (Vital River Laboratories, Beijing, China). Starting from the first week after injection, tumor size was measured every three days until 5 weeks. The tumor volumes were calculated using the formula: $V = 0.5 \times ab^2$, where a and b represent the length and width of the tumor, respectively. After 5 weeks, mice were sacrificed and tumor tissues were harvested for further analysis. All animal protocols were approved by the Ethics Committee of Luoyang Orthopedic-Traumatological Hospital.

Immunohistochemistry

Immunohistochemical staining was carried out using the S Pl ink Detection Kit (Zsbio, Beijing, China). Briefly, the paraffin-embedded sections were deparaffinned in xylene and dehydrated in a graded series dilution of alcohol before antigen retrieval in EDTA. After incubation with 3% H_2O_2 in methanol for 15 min to quench endogenous peroxidase, the tissue sections were blocked by goat serum for 30 min, and incubated with primary antibodies [EMP3 (ab236671, Abeam, 1:1000 dilution), phospho-ERK (ab223500, Abcam, 1:1000 dilution) and E-cadherin (ab76055, Abeam, 1:500 dilution)] at 4° C overnight and biotinylated secondary antibody for 30 min at room temperature. The diaminobenzidine solution was used to detect proteins of interest. The sections were finally counterstained with hematoxylin, mounted with Histomount (ThermoScientific) and photographed with an Olympus bright- field microscope. The antibodies and the dilutions used for immunohistochemistry were listed below:EMP3 (ab236671, Abcam, 1:1000 dilution), p-c-

RAF (ab225628, Abcam, 1:500 dilution), MEK (ab32091, Abcam, 1:1000 dilution), phospho-MEK (ab278564, Abcam, 1:1000 dilution), ERK (ab184699, Abcam, 1:1000 dilution), phospho-ERK (ab223500, Abcam, 1:1000 dilution), GAPDH (ab8245, Abcam, 1:1000 dilution). The secondary antibodies used in this study include: anti-mouse IgG H&L (ab150113, Abcam, 1:10000 dilution), anti-rabbit IgG H&L (ab150077, Abcam, 1:10000 dilution).

Statistics

Statistical analyses were performed by SPSS 21.0 software (SPSS Inc., Chicago, IL). All data were presented as mean ± standard deviation (SD). The two-tailed student's t-test was performed for comparisons between two groups. The Kaplan-Meier method with Log-rank test was used to compare the survival rate of OS patients. Linear correlation was evaluated by Person correlation analysis. The Chi-square test was used to analyze the correlation between clinicopathological features of OS patients and Circ-DNAH1 expression. $P < 0.05$ was considered statistically significant.

RESULTS

Circ-DNAH1 expression is significantly down-regulated in OS and lower levels of circ-DNAH1 predicts poor prognosis

To find the dysregulated circRNAs, we screened a dataset deposited by one previous study on mapping differentially expressed circRNAs between seven human osteosarcoma cell lines (U2OS, U20S/MTX300, MG63, HOS, 143B, ZOS and ZOS-M) and one human osteoblast hFOB1.19 cells in GEO database (https://www.ncbi.nlm.nih.gov/geo/geo2r/?acc=GSE96964) [20]. We found that has_circ_l04892 was down-regulated in the OS and was one of the most significant differentially expressed circRNAs with the lowest *P*value (Figure 1A). qRT-PCR analysis confirmed that the expression of has_circ_l04892 was significantly suppressed ($P < 0.05$) in five OS cell lines (HOS, 143B, Saos2, MG63 and U2OS) compared with the hFOBl.19 cells (Figure 1B). Furthermore, qRT-PCR analysis of has_circ_l04892 expression in 60 pairs of OS tumor tissues and the adjacent noncancerous tissues showed that the abundance of has_circ_l04892 was markedly reduced by 2~3 fold ($P < 0.001$) in OS (Figure 1C). Then based on the median expression of hsa_circ_104892 in all OS patients, we divided the OS patients into a low and a high hsa_circRNA_l04892 expression group ($n = 30$). The Kaplan-Meier analysis revealed that the OS patients of low hsa_circ_l04892 expression group were more likely to develop recurrence and have poor disease-free survival ($P < 0.001$; Figure 1D).

Chi-square test demonstrated that hsa_circ_104892 expression was strongly correlated ($P < 0.05$) with the tumor size, TNM staging and lymph node metastasis, but not with the age, sex and tumor differentiation in OS patients (Table 1). Our univariate Cox regression dialysis also showed that hsa_circ_104892 level, TNM staging and lymph node metastasis, but not the age, sex and tumor size, were reliable predictors ($P < 0.05$) for the prognosis of OS patients ($P < 0.05$, Table 2). Multivariate Cox analysis confirmed that the hsa_circ_104892 expression and TNM staging served as independent factors for predicting the OS patient survival ($P < 0.05$, Table 2).

Circ-DNAH1 is derived from *DNAH1* gene exon 67-70 and is predominately localized in the cytoplasm

RNA sequencing indicated that hsa_circRNA_l04892 was generated from the exons of 67 to 70 in the human *DNAH1* gene (chr3:c2394464-52395678) through back splicing (Figure 2A). For clarity, we termed hsa_circRNA_104892 as circ-DNAH1 hereafter. Without poly(A) tails, circRNAs are more stable than the linear mRNAs. Therefore, we treated the two OS cell lines, MG63 and U2OS (which exhibited a moderate level of circ-DNAH1 expression) with Actinomycin D, a well-known inhibitor for linear RNA transcription. qRT-PCR analysis showed that the circ-DNAH1 level in MG63 and U2OS cells was not significantly changed, while the level of DNAH1 mRNA was markedly decreased 4 to 24 hours after Actinomycin D treatment (Figure 2B, 2C). To confirm the circular nature of circ-DNAH1, we treated the total RNAs from MG63 and U2OS cells with RNase R that has a 3'-5' exoribonuclease activity. Compared to the linear DNAH1 mRNA, circ-DNAH1 was completely recalcitrant to RNase R digestion (Figure 2D, 2E). To analyze the intracellular location of circ-DNAH1, we fractionated the nucleus and cytoplasm of MG63 and U2OS cells. qRT-PCR analysis showed that circ-DNAH1 was primarily detected in the cytoplasm fraction, suggesting DNAH1 is mostly concentrated in cytoplasm (Figure 2F, 2E). Moreover, FISH analysis confirmed the cytoplasmic location of circ-DNAH1. U6 and 18S RNA, RNA markers for the nucleus and cytoplasm respectively, were detected at their respective locations in MG63 and U2OS cells (Figure 2H). In addition,, circular DNAH1 and linear DNAH1 were positive correlated with each other, indicating that they have the same origin (Supplementary Figure 2).

Circ-DNAH1 inhibits proliferation, migration and invasion of OS cells cultured *in vitro*

The inverse correlation between the abundance of circ-DNAH1 and tumor development suggests that circ-

DNAH1 functions as a tumor suppressor in OS development. To further characterize the functional role of circ-DNAH1, we overexpressed or silenced circ-DNAH1 in MG63 and U2OS cells. qRT-PCR analysis showed that circ-DNAH1, but not DNAH1, was overexpressed in MG63 and U2OS cells transfected with pcDNA3.1 circ-DNAH1 (Figure 3A). Similarly, the level of circ-DNAH1, but not that of DNAH1, was significantly reduced in MG63 and U2OS cells transfected shRNA_circ-DNAH1 compared with transfection with the control shRNA (Figure 3B). CCK-8 proliferation assay indicated that while the overexpression of circ-DNAH1 significantly slowed the proliferation of MG63 and U2OS cells, silencing of circ-DNAH1 accelerated it (Figure 3C, 3D). Moreover, transwell without matrix gel and *in vitro* scratch assays revealed that overexpression and silencing of circ-DNAH1 significantly weakened and facilitated the migration of MG63 and U2OS cells, respectively (Figure 3E–3H). Similarly, Transwell assays with matrix gel revealed that overexpression and silencing of circ-DNAH1 significantly decreased and increased the invasion ability of MG63 and U2OS cells, respectively (Figure 3I, 3J).

Circ-DNAH1 sponges miR-663a in OS cells

RNA motif prediction by RegRNA 2.0 identified that circ-DNAH1 contained four putative binding sites to bind to miR-663a (Figure 4A). To verify these binding sites, we first used a luciferase reporter assay to confirm that wild type

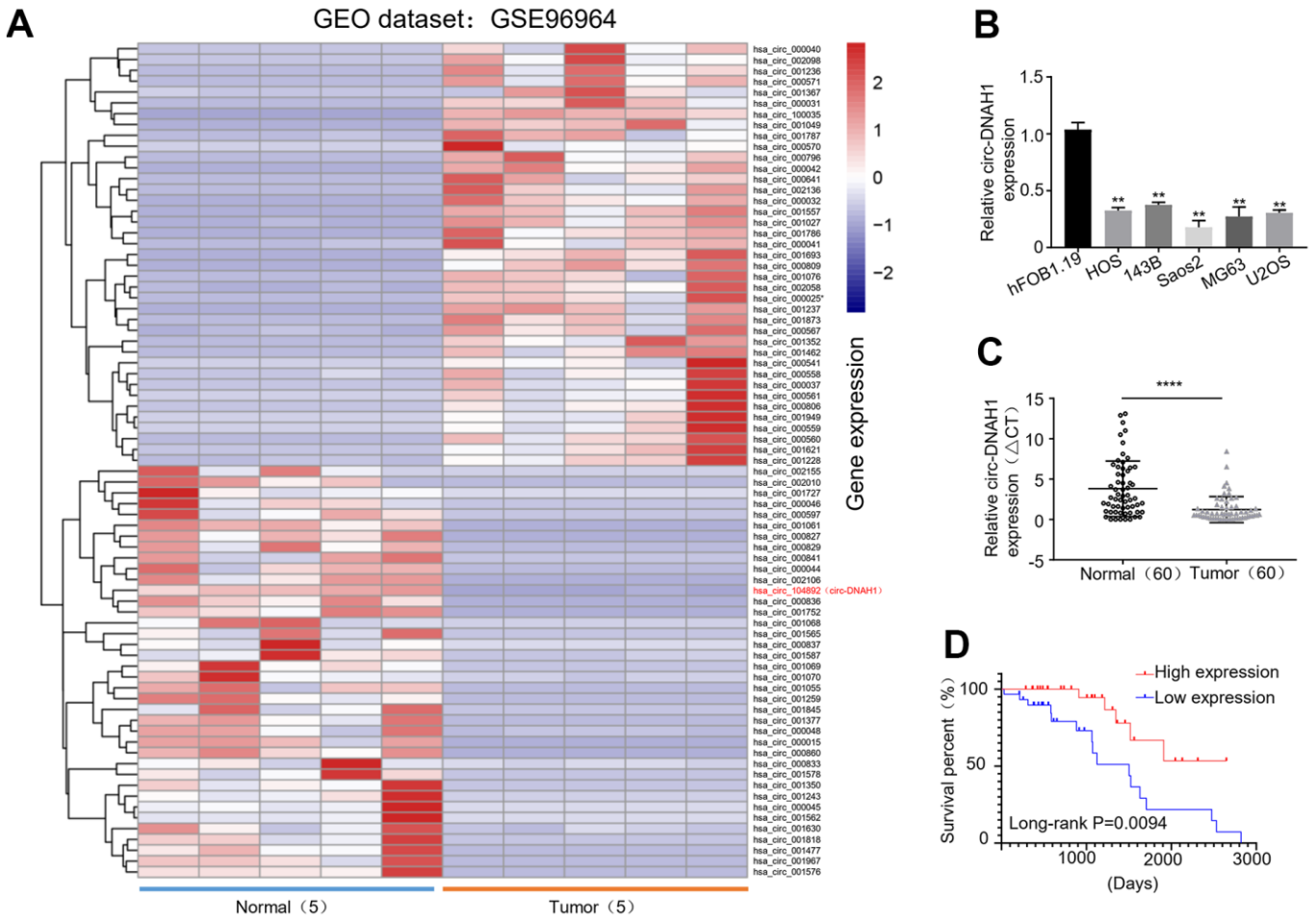

Figure 1. hsa_circRNA_104892 expression is significantly downregulated in OS and decreased circ- hsa_circRNA_104892 expression predicts poor prognosis. (**A**) Hierarchical clustering heat map showing the top 250 differentially expressed circular RNAs in OS cell lines versus human osteosarcoma in the order of significance based on *P* value, with hsa_circRNA_l04892 on the very top. Data is retrieved from the GEO database (GSE96964). (**B**) qRT-PCR analysis of hsa_circRNA_l04892 expression in HOS, 143B, Saos2, MG63, U2OS and hFOB1.19 cells. Data we shown as mean ± SD. ***P* < 0.01. (**C**) qRT-PCR analysis of has_circRNA_l04892 expression from 60 OS tumor tissues paired with the adjacent noncancerous tissues. (**D**) Kaplan-Meier analysis of the survival rate of OS patients with low and high hsa_circRNA_l04892 expression (*n* = 30 in each group). Data are shown as mean ± SD. ***P < 0.001.

Table 1. Chi-square analysis of hsa_circRNA_104892 expression with demographic and pathological factors of OS patients.

Clinicopathological characteristics	Total	circ-DNAH1 high expression (n=30)	circ-DNAH1 low expression (n=30)	X^2	P value
Gender					
male	31	17	14	0.601	0.438
female	29	13	16		
Age					
<=25	27	14	13	0.67	0.795
>25	33	16	17		
Tumor size					
T1	18	12	6	9.654	0.022
T2	14	8	6		
T3	9	6	3		
T4	19	4	15		
Differentiation					
high	16	10	6	1.800	0.407
moderate	20	8	12		
poor	24	12	12		
Lymph node metastasis					
Positive	16	9	17	4.344	0.037
Negative	34	21	13		
TMN stages					
I	16	12	4	8.800	0.032
II	15	9	6		
III	9	3	6		
IV	20	6	14		

Table 2. Univariate and multivariate Cox regression analysis of the prognostic factors of OS patients.

Overall survival	B	SE	Wald	df	P value	Exp(B)	95%Exp(B)	
							Upper limit	Lower limit
circ-DNAH1	1.277	0.629	4.117	1	0.042	3.586	1.044	12.315
Tumor differentiation	0.21	0.412	0.259	1	0.1351	1.254	0.55	2.854
TMN stage	-1.473	0.489	9.08	1	0.003	0.229	0.088	0.598
Lymphatic metastasis	-1.237	0.459	8.72	1	0.035	1.984	0.605	0.998
Tumor size	-0.115	0.182	0.398	1	0.528	0.897	0.624	1.274
Sex	-0.002	0.016	0.017	1	0.895	0.998	0.967	1.03
Age	-0.275	0.51	0.292	1	0.589	0.759	0.28	2.062

circ-DNAH1 mitigated the expression of miR-663a luciferase reporter. Site-directed mutagenesis was then performed to successively mutate each potential binding site. While the mutant of four potential binding sites (circ-DNAH1-MUT) abolished the inhibitory effect of circ-DNAH1 on miR-663a expression (Figure 4A, 4B), a single binding site mutant partially reversed the inhibition of circ-DNAH1 (Supplementary Figure 1). Both circRNAs and miRNAs are known to completely bind to Ago2, through which sponge takes place[14, 22]. In both MG63 and U2OS cells, immunoprecipitation with anti-Ago2 antibody significantly enriched more circ-DNAH1 and miR-663a compared with the control, IgG antibody (Figure 4C, 4D). Then, we labeled circ-DNAH1 with biotin using *in vitro* transcription, and performed RNA pulldown experiments to identify the

microRNA that was sponged by circ-DNAH1 from the homogenates of MG63 and U2OS cells. The biotin-labeled circ-DNAH1, not the biotin control, recovered significant amount of miR-663a, thus demonstrating the direct binding between circ-DNAH1 and miR-663a *in vitro* (Figure 4E, 4F).

Next, we expressed the biotinylated miR-663a and biotinylated miR-663a-MUT in MG63 and U2OS cells. RNA pull-down experiment showed that significant amount of circ-DNAH1 bound to the biotinylated miR-663a, but not to biotinylated miR-663a-MUT or the biotin control, thus demonstrating a direct interaction between circ-DNAH1 and miR-663a *in vivo* (Figure 4G, 4H). Moreover, FISH analysis revealed that circ-DNAH1 was co-localized with miR-663a in MG63 cells (Figure 4I).

MiR-663a is up-regulated in OS, and promotes OS progression through multiple downstream targets

Having demonstrated miR-663a is the target of circ-DNAH1, we wondered what was the function of miR-663 in OS progression. To answer this, we first used qRT-PCR to examine the expression level of miR-663 in OS tissues and cell lines. Compared with the adjacent noncancerous tissues, the level of miR-663a was markedly increased by 2.3-fold ($P < 0.001$) in OS tumor

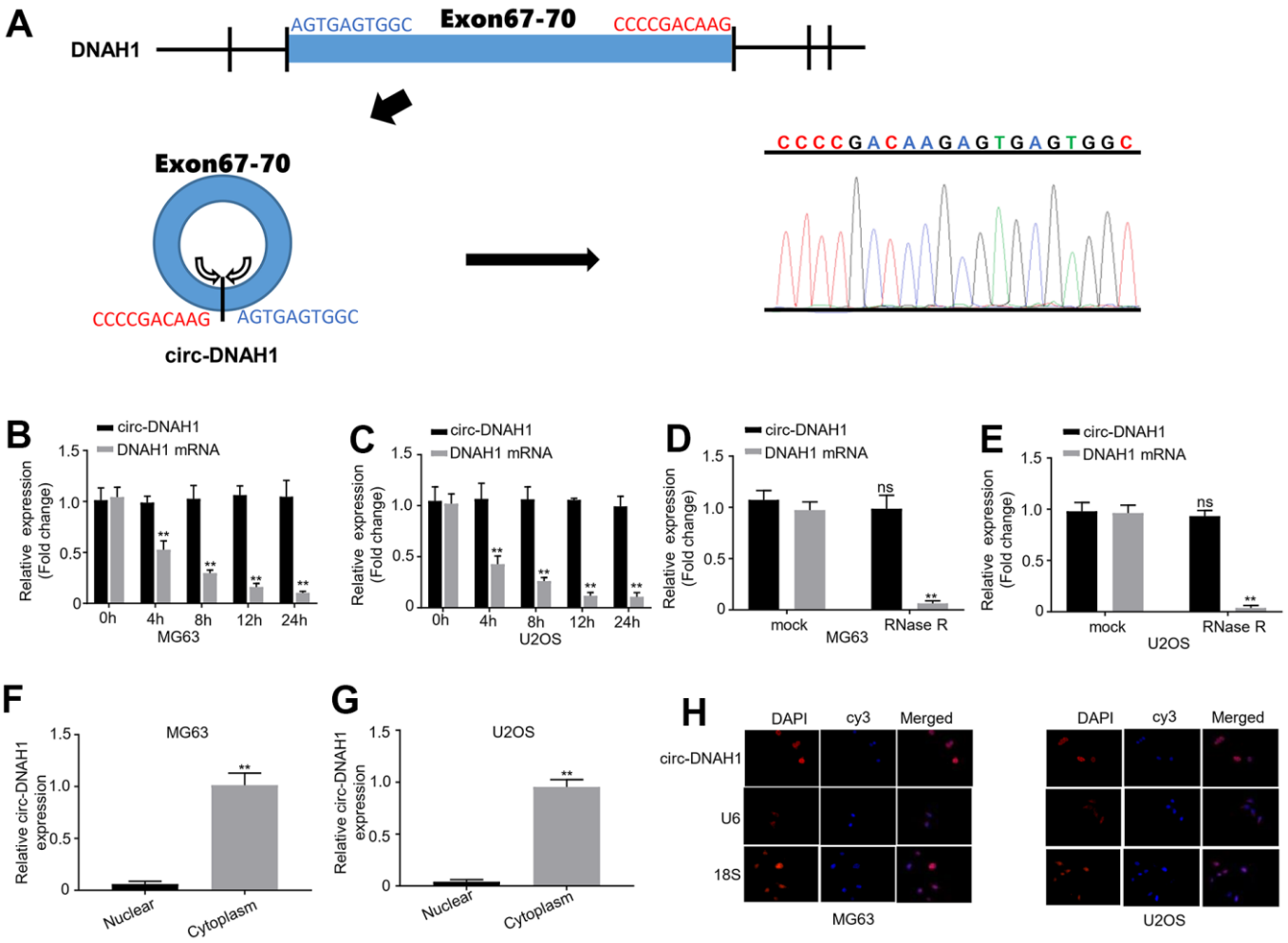

Figure 2. Circ-DNAH1 is derived from the DNAH1 gene exon 67-70 and predominately localized in the cytoplasm. (**A**) Schematic illustration of the generation of circ-DNAHI from the exons 67 to 70 of the *DNAH1* genome by back splicing. The immediate DNA sequence from the splice donor and splice acceptor sites was indicated (left), and was confirmed by the data from RNA sequencing (right). (**B**, **C**) qRT-PCR analysis of circ-DNAH1 and DNAH1 mRNA expression in MG63 and U2OS cells treated with Actinomycin D for different time (0 h, 4 h, 8 h, 12 h and 24 h). (**D**, **E**) Quantification of circ-DNAH1 and DNAH1 mRNA in total RNA of MG63 and U2OS cells digested with or without RNase R. (**F**, **G**) qRT-PCR analysis of the abundance of circ-DNAH1 and DNAH1 mRNA in the nuclear and cytoplasmic fractions isolated from MG63 and U2OS cells, (**H**) FISH analysis of circ- DNAH1 in the MG63 and U2OS. U6 and 18S RNA were stained by fluorescent probe as well. Data we shown as mean ± SD. $^{**}P < 0.01$ and ns = no significance.

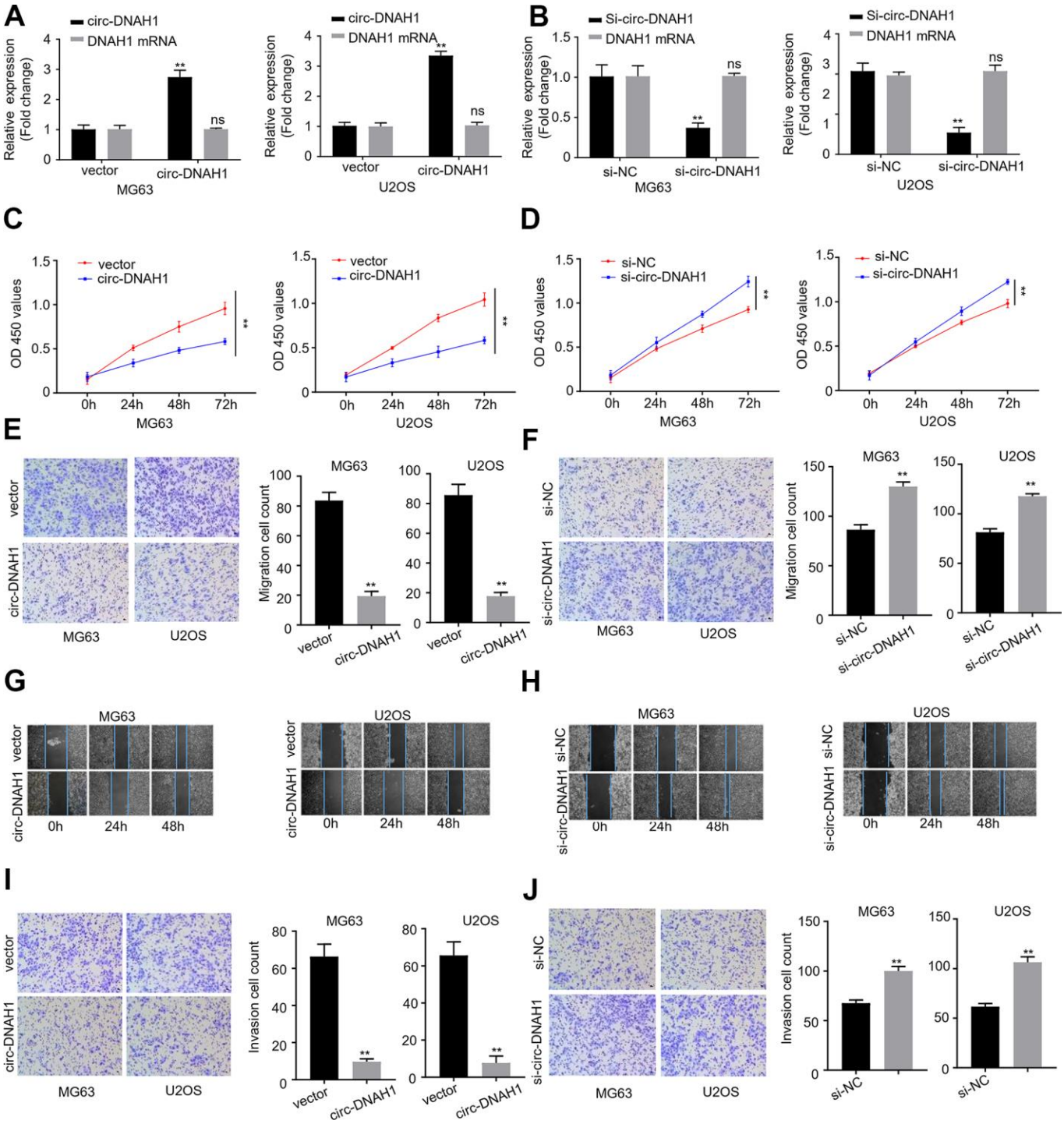

Figure 3. Circ-DNAH1 inhibits proliferation, migration and invasion of OS cells *in vitro.* (**A**, **B**) qRT-PCR analysis of circ-DNAH1 and DNAH1 mRNA expression in MG63 and U2OS cells infected with recombinant lentivirus, LV-circ-DNAH1 (**A**) or LV-circ-DNAH1 shRNA-1/2 (**B**). (**C**, **D**) The MG63 and U2OS cells were infected with recombinant lentivirus, LV-circ-DNAH1 (**C**) or LV-circ-DNAH1 shRNA-1/2 (**D**), and cell proliferation was measured at Oh, 24h, 48h and 72h. (**E**, **F**) Transwell migration assay of MG63 and U2OS cells infected with recombinant lentivirus, LV-circ-DNAH1 (**E**) or LV-circ- DNAH1 shRNA-1/2 (**F**). (**G**, **H**) *In vitro* scratch migration assay of MG63 and U2OS cells infected with recombinant lentivirus, LV-circ-DNAH1 (**G**) or LV-circ-DNAH1 shRNA-1/2 (**H**). (**I**, **J**) Transwell invasion assay of MG63 and U2OS cells infected with recombinant lentivirus, LV-circ- DNAH1 (**I**) or LV-circ-DNAH1 shRNA-1/2 (**J**). Data are shown as mean ± SD. $^{**}P < 0.01$ and ns = no significance.

tissues (Figure 5A). Similarly, miR-663a expression was higher ($P < 0.05$) in five OS cell lines (HOS, 143B, Saos2, MG63 and U2OS) than in hFOB1.19 cells (Figure 5B). To further explore the role of miR-663a in OS progression, we divided the OS patients into low and high miR-663a expression groups according to miR-663a median expression level. The Kaplan-Meier analysis showed that the high-miR-663a-expression group more likely developed recurrence and had poorer disease-free survival ($P < 0.001$; Figure 5C). CCK-8

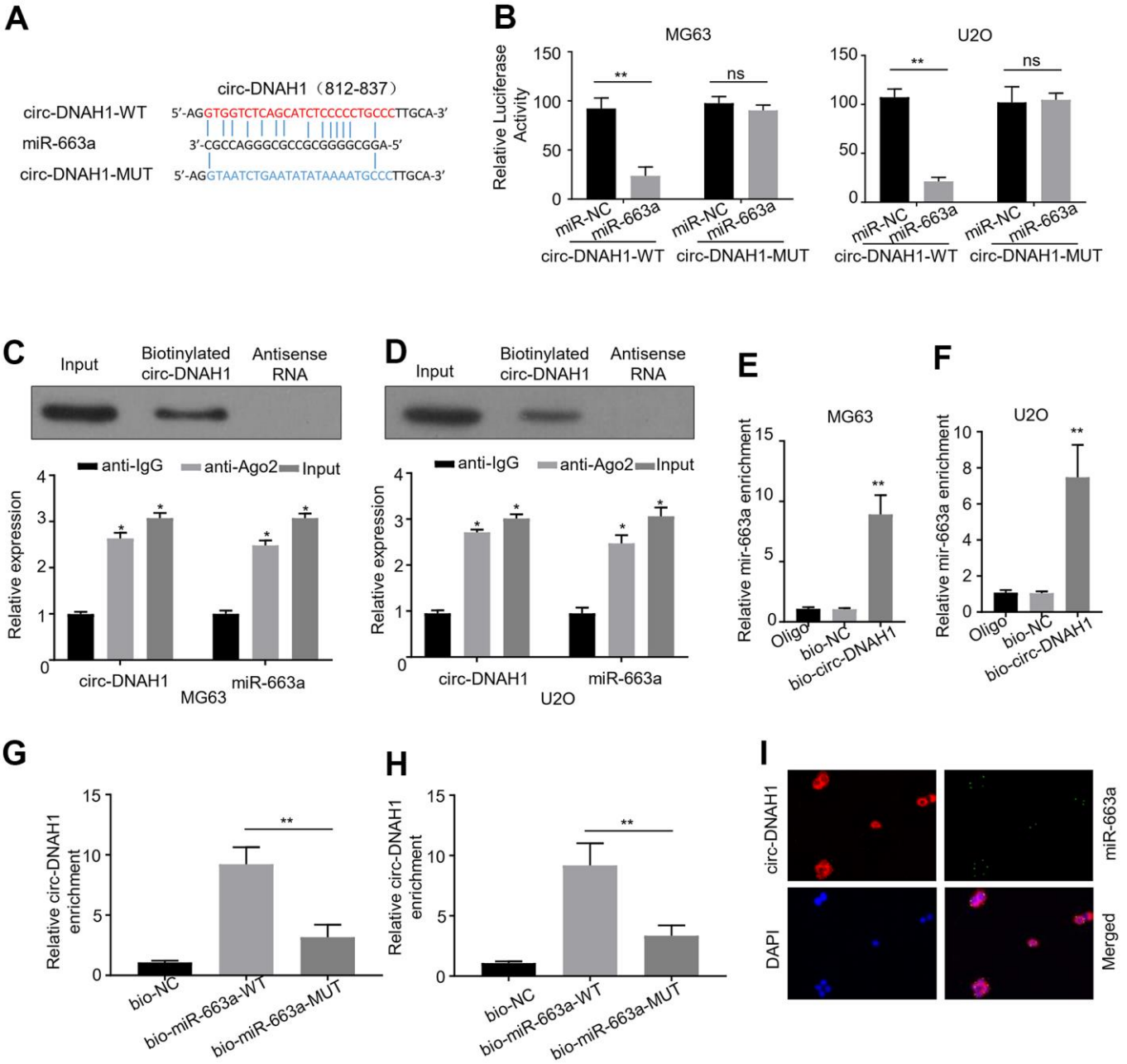

Figure 4. Circ-DNAH1 sponges miR-663a in OS cells. (**A**) Four potential binding sites for miR-663a in a conserved locus of Circ-DNAH1 were identified. In the construct cire-DNAH1-MUT, the four putative binding sites were mutated, (**B**) Luciferase reporter analysis of MG63 and U2OS cells transfected with wild-type (circ-DNAH1 WT) and circ-DNAH1 MUT. Note that circ-DNAH1-MUT completely reversed the inhibitory effect of circ-DNAH1 on miR-663a expression. (**C**, **D**) Immunoprecipitation with the anti-Ago2 antibody from MG63 and U2OS cell extracts, followed by qPCR analysis of circ-DNAH1 and miR-663a. (**E**, **F**) RNA pull-down analysis of the homogenates of MG63 and U2OS cells using a biotin-labeled circ-DNAH1 and streptavidin detection, followed by qPCR analysis of miR-663a. (**G**, **H**) The biotinylated miR-663a and biotinylated miR-663a-MUT were transfected in MG63 and U2OS cells. RNA pull-down experiment was performed, followed by qPCR analysis of circ-DNAH1. (**I**) FISH dialysis of circ-DNAH1 (red) and miR-663a in MG63 cells, with DAP I (blue) counterstaining the nucleus.

proliferation assay found that the expression of miR-663a mimics significantly strengthened the proliferation of MG63 and U2OS cells, while expression of miR-663a inhibitor undermined the OS cell proliferation (Figure 5D, 5E). Furthermore, transwell assays with and without matrix gel indicated that the expression of miR-663a mimics significantly increased the abilities of migration and invasion of OS cells, but the expression of miR-663a resulted in an opposite phenotype (Figure 5D, 5E). Collectively, these data confirmed that miR-663a functions as an oncogene in OS development *in vitro*.

Recently, epithelial membrane protein-3 (EMP3) was shown to be downregulated in human gallbladder cancer and inhibited the tumor growth by modulating mitogen-activated protein kinase (MAPK)/extracellular regulated protein kinases (ERK) signaling [21]. Interestingly, EMP3 is the downstream target gene of miR-663a. To validate whether EMPs was a target of miR-663a in OS, we examined the expression and phosphorylation of EMP3 and ERK 1/2 by western lotting in OS cells (Figure 5J, 5K). In addition, we checked the phosphorylation of MEK and c-Raf that are principal components of the ERK 1/2 signaling pathway. The presence of miR-663a mimics moderately increased the level of EMP3 as well as the phosphorylation of MEK, ERK and c-Raf in MG63 and U2OS cells, while the presence of miR-663a inhibitor decreased EMP3 level as well as the phosphorylation of MEK, ERK and c-Raf. Collectively, these data suggest that circ-DNAH1 and miR-663a can regulate the OS tumor growth through EMP3 and MAPK/ERK pathway.

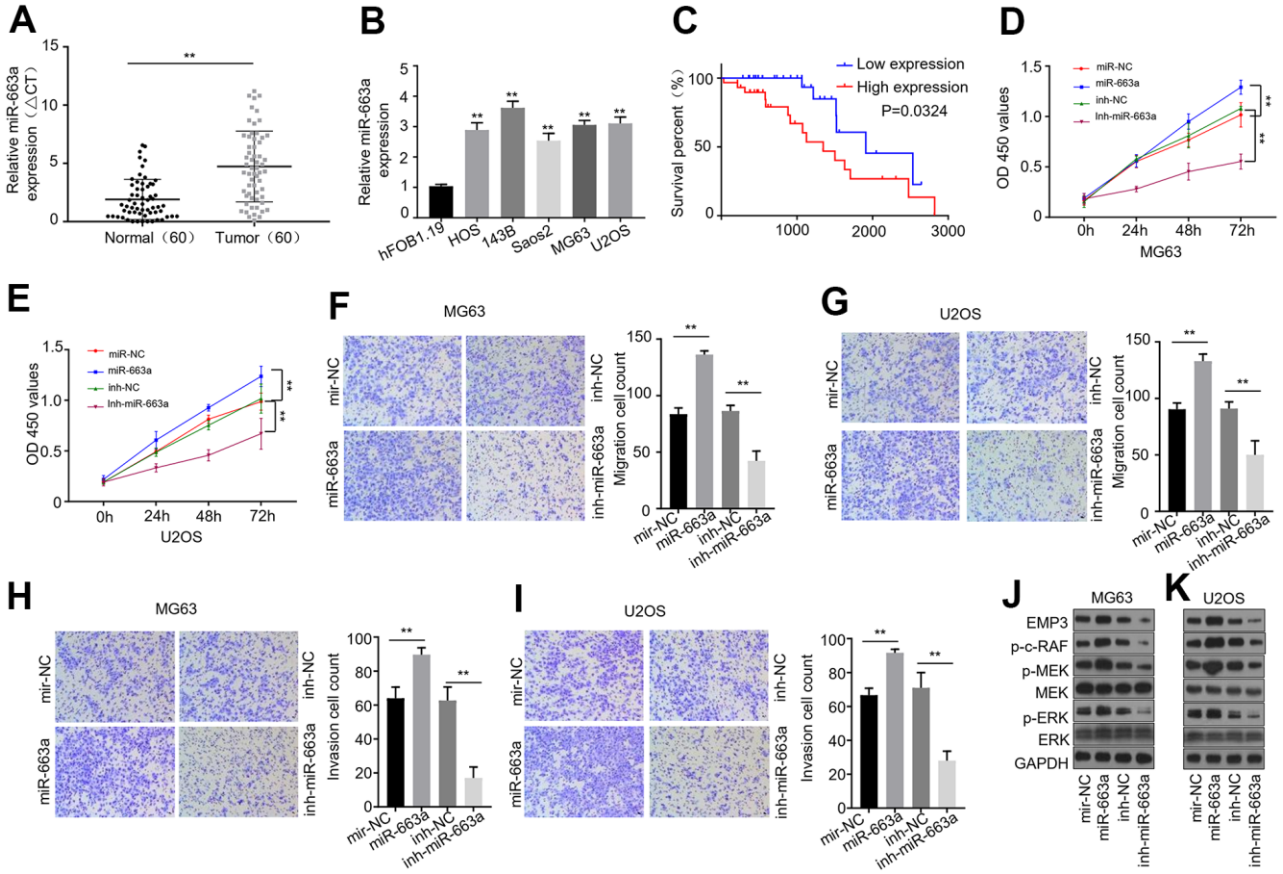

Figure 5. miR-663a is up-regulated in OS tissues and cell lines, and promotes OS progression through targeting EMP3 *in vitro*. (**A**) qPCR analysis of miR-663a expression in OS tumor tissues and the adjacent noncancerous tissues (n = 60). (**B**) qPCR dialysis of miR-663a expression in HOS, 143B, Saos2, MG63, U2OS and hFOB1.19 cells. (**C**) The Kaplan-Meier analysis of disease-free survival of the low and high miR-663a expression groups. (**D**, **E**) CCK-8 cell proliferation assay of MG63 and U2OS cells expressing miR-663a mimics or miR-663a inhibitor. (**F**, **G**) Transwell migration assays of MG63 and U2OS cells expressing miR-663a mimics or miR-663a inhibitor. (**H**, **I**) Transwell invasion assays of MG63 and U2OS cells expressing miR-663a mimics or miR-663a inhibitor. (**J**, **K**) Immunoblotting analysis of EMP3, MEK and ERK, as well as pMEK, pERK and p-c-Raf in MG63 and U2OS cells expressing miR-663a mimics or miR-663a inhibitor. GAPDH serves as a loading control. miR-NC and inh-NC: negative controls for miR-663a mimics and miR- 663a inhibitor, respectively. Data are shown as mean ± SD. $^{**}P < 0.01$ and ns = no significance.

Overexpression of circ-DNAH1 reverses miR-663a-induced enhancement of cell proliferation, migration and invasion of OS cells

Next, we further characterized the interaction between circ-DNAH1 and miR- 663a using transfection and function assays in MG63 and U2OS cells. qRT-PCR analysis confirmed that overexpression of circ-DNAH1 in MG63 and U2OS cells reduced the level of the endogenous miR-663a, while silencing of circ-DNAH1 led to an increase of miR-663a (Figure 6A). Spearman correlation analysis showed that there was a significant inverse correlation (Spearman r > 0.6, $P < 0.001$) between the levels of circ-DNAH1 and miR-663a in 60 cases of OS patients (Figure 6B). Functionally, overexpression of miR-663a promoted the cell growth, migration and invasion of MG63 and U2OS cells, which was abolished by the combination of circ-DNAH1 overexpression, as demonstrated by the CCK8 proliferation and transwell experiments (Figure 6C–6E). Immunoblotting analysis also showed that overexpression of miR-663a promoted the expression of EMP3, and the phosphorylation of c-Raf, MEK and ERK in MG63 and U2OS cells, and these effects were reversed by circ-DNAH1 overexpression (Figure 6F). Collectively, these results confirmed that circ-DNAH1 functions as an antagonist for miR-663a in OS cells.

Enforced expression of circ-DNAH1 suppresses OS growth and metastasis *in vivo*

Finally, we tested the effect of circ-DNAH1 overexpression on OS cell proliferation *in vivo* using the

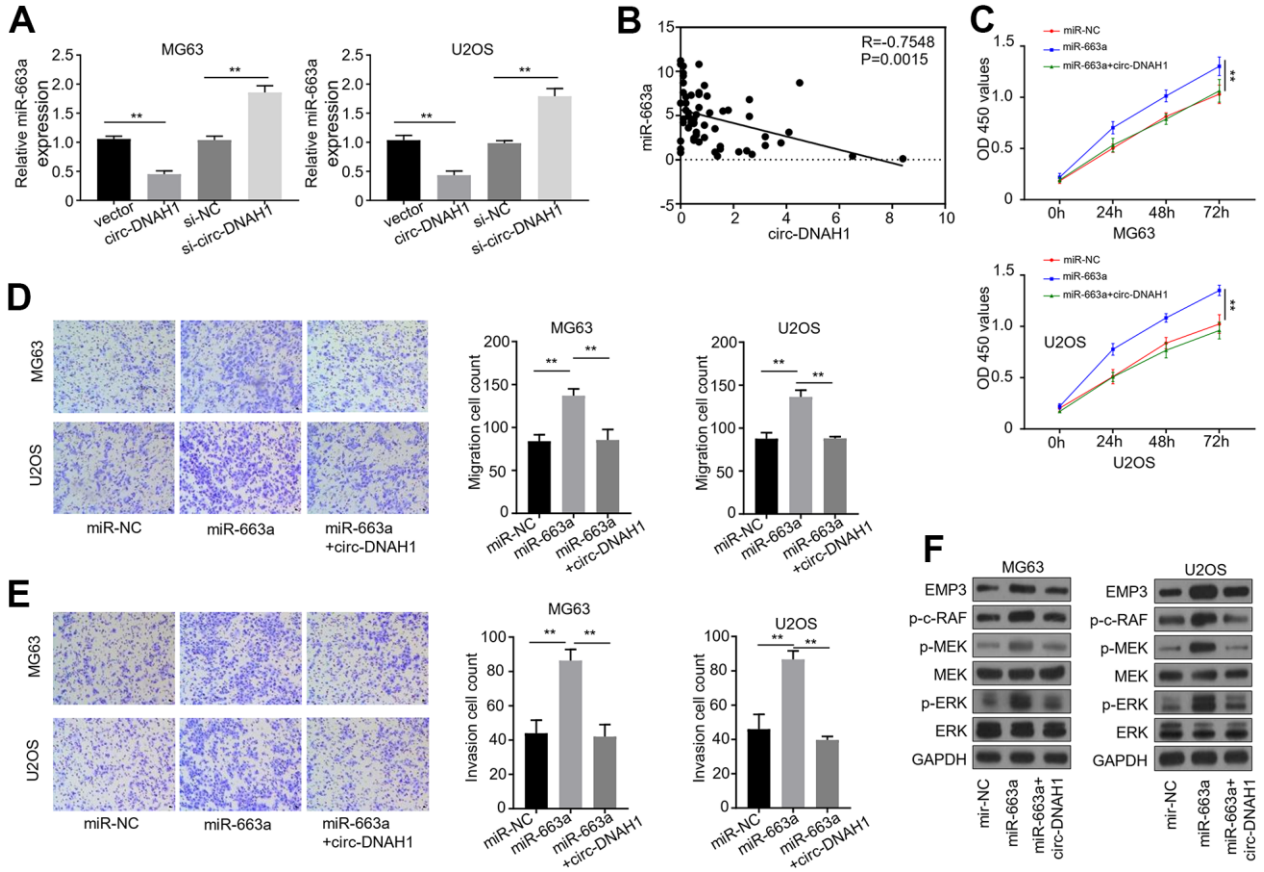

Figure 6. Over-expression of circ-DNAH1 reverses miR-663a-induced enhancement of cell proliferation, migration and invasion in OS cells. (**A**) qRT-PCR quantification of miR-663a in MG63 and U2OS cells transfected with circ-DNAH1 or siRNAs against circ-DNAH1 (si-circ-DNAH1). (**B**) Spearman correlation analysis of the circ-DNAH1 and miR-663a levels in 60 cases of OS patients, (**C**) CCK-8 cell proliferation assay of MG63 and U2OS cells expressing miR-663a mimics or miR-663a mimics in combination with circ-DNAH1. (**D**) Transwell migration assays of MG63 and U2OS cells expressing miR-663a mimics or miR-663a mimics in combination with circ-DNAH1. (**E**) Transwell invasion assays of MG63 and U2OS cells expressing miR-663a mimics or miR-663a mimics in combination with circ-DNAH1. (**F**) Immunoblotting analysis of EMP3, MEK and ERK, as well as pMEK, pERK and p-c-Raf in MG63 cells expressing miR-663a mimics or miR-663a mimics in combination with circ-DNAH1. GAPDH serves as a loading control. miR-NC: negative controls for miR-663a mimics. Data are shown as mean ± SD. $^{**}P < 0.01$ and ns = no significance.

nude mice tumor transplant model. MG63 and U2OS cells stably transfected with circ-DNAH1 were subcutaneously injected into the breast fat pads of nude mice. Starting from as early as 1 week and progressing to 5 weeks, the volume of xenograft was significantly reduced by circ-DNAH1 overexpression (Figure 7A). Immunohistochemistry further showed that the expression of Ki-67, a marker for cell proliferation, were significantly suppressed in the OS cells overexpressing circ-DNAH1 but not in control cells (Figure 7B). Moreover, circ-DNAH1 overexpression increased the expression of EMP3 and E-cadherin (Figure 7B). E-cadherin is critically involved in tumor cell migration, invasion and metastasis [22], and the loss of E-cadherin has been associated with greater tumor metastasis [23]. Interestingly, circ-DNAH1 overexpression also reduced the phosphorylation of ERK, resulting in the inactivation of MAPK/ERK signaling (Figure 7B). Collectively, the increase of the expression of EMP3 and E-cadherin as well as the inhibition of cell proliferation and MAPK/ERK signaling induced by circ-DNAH1 overexpression indicates that circ-DNAH1 acts as a tumor suppressor *in vivo*.

DISCUSSION

Although post-surgery neoadjuvant chemotherapy and adjuvant chemotherapy has been widely used for OS treatment [24], the results from clinical trials suggest that the survival rate could not be further improved by the clinical efforts such as adjusting dosage and reducing the cytotoxicity of chemotherapy [25]. For example, OS patients with lung and bone metastasis perform poorly in overall survival and event-free survival after post-surgery chemotherapy. OS patients with tumor in the axial skeleton also generally have poor prognosis, as the OS in appendicular skeleton is more difficult to remove by surgery. Despite that metastasis is only found in 10-20% of OS patients at the time of diagnosis, up to 90% of OS patients likely have sub clinical or undetectable micro-metastatic sites. To date, the examination of OS metastasis mainly resorts to computed tomography, chest X-ray, bone scan and biopsy, but without reliable biomarkers, these approaches are less sensitive. Thus, development of novel biomarkers that reliably reflect OS proliferation and metastasis would greatly benefit OS diagnosis and treatment.

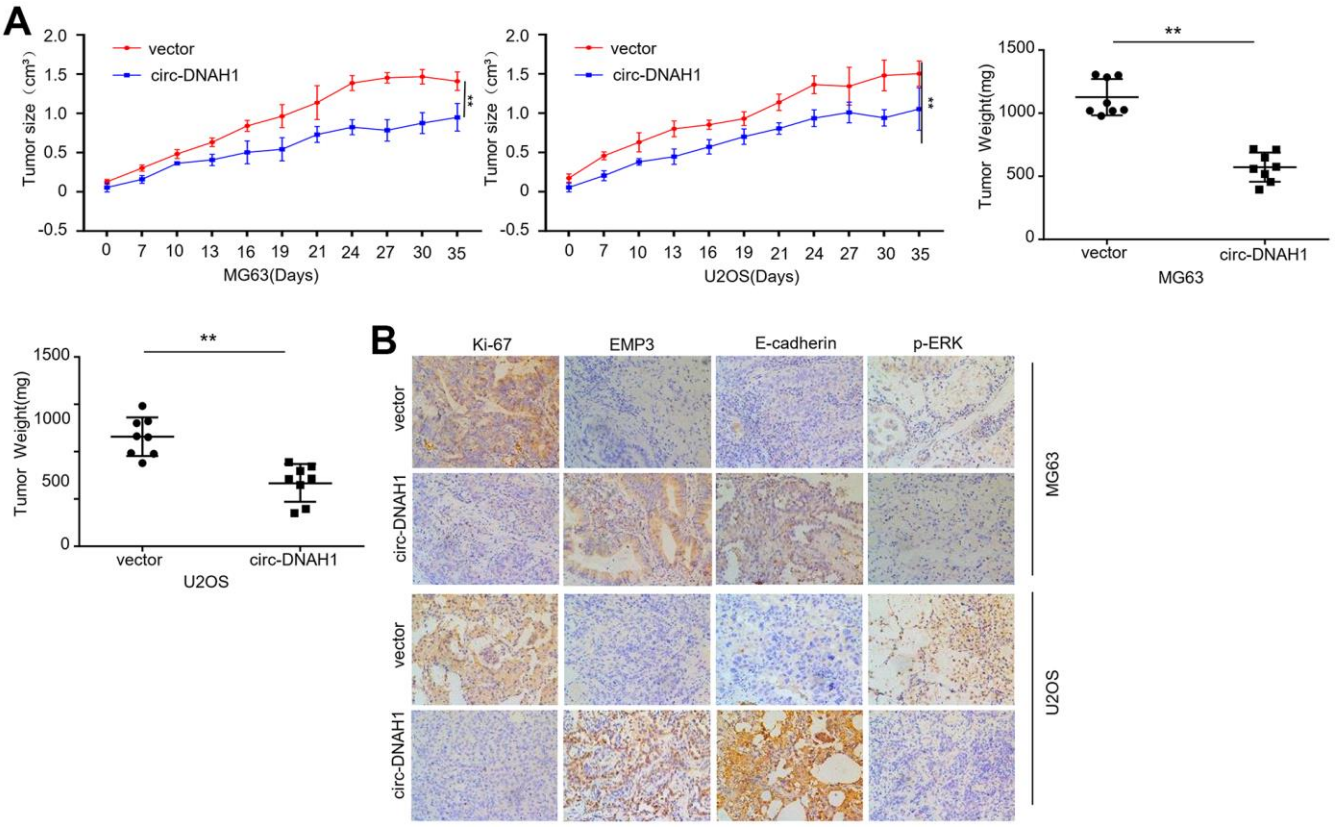

Figure 7. Enforced expression of circ-DNAH1 suppresses OS growth and metastasis *in vivo*. (**A**) The volume of tumor xenograft formed by MG63 and U2OS cells overexpressing circ- DNAH1 or vector control, (**B**) Immunohistochemistry analysis of ki-67, EMP3, E-cadherin and p-ERK. Data are shown as mean ± SD. ***P* < 0.01 and ns = no significance.

On the other hand, the stagnation in clinical progress makes the basic research into the molecule mechanisms of OS development more imperative. However, our understanding of the OS etiology lags behind the studies on the etiology of other cancer types. Other than p53 and RBI that are proposed to act as oncogenic drivers, pre-existing genomic instability, PTEN loss and DNA methylation may also contribute to OS tumorigenesis and relapse [26]. In addition, a number of prognostic markers have been reported, including single nucleotide polymorphism (SNP) variants in the nuclei factor I/B gene (NFIB) gene [27] and microRNAs. Interestingly, one recent study suggested that circulating miR-663a, the microRNA that we found in this study, is a potential biomarker for diagnosing OS [28].

CircRNAs have been shown to regulate tumorigenesis in a number of cancers [29]. Due to the high abundance and stability, CDR1as, which increases the expression levels of miR-7 target genes by suppressing miR-7 activity, is involved in many different human cancers. In addition to CDR1as, cireFoxo3 promotes cell apoptosis through interactions with p53 and MDM2; in contrast, circRNAs derived from TTBK2 and UBAP2 inhibit apoptosis [30–32]. These findings indicate that circRNAs are functionally versatile in cancer progression.

Recently, circUBAP2, circ-0016347 and CDR1as have been reported to be upregulated in OS tissues and sponge miR-143, miR-214 and miR-7, respectively, through which the three circRNAs promote OS progression, and thus act as oncogenes [17–19]. One micro array study examining the differentially expressed circRNAs between human osteosarcoma cell lines and human osteoblasts provided an opportunity to functionally characterize the key circRNAs involved in OS progression [20]. We analyzed the data deposited in the GEO database, and found that a novel cytoplasmic circRNA, circ-DNAH1, is significantly downregulated in OS cancer tissues and OS cell lines. Importantly, the low levels of circ-DNAH1 are inversely correlated with overall survival. Thus, circ-DNAH1 expression could be used as an independent prognostic factor for OS patients. It would be of great interest to examine whether circ-DNAH1 can be detected from circulating blood, as circRNAs-containing exosomes have been reported in multiple cancers. Functionally, overexpression of circ-DNAH1 inhibits the proliferation, migration and invasion of OS cells *in vitro*. Mechanistically, circ-DNAH1 sponges miR-663a that functions as an oncogene and promotes OS progression through EMP3 and MAPK/ERK signaling pathway. Overexpression of circ-DNAH1 reverses miR-663a-induced enhancement of cell proliferation, migration and invasion of OS cells. Furthermore, overexpression of circ-DNAH1 suppresses OS growth and metastasis *in vivo*. Our findings together with other studies on circRNAs in OS demonstrate that multiple circRNAs differentially regulate cancer development by acting as either oncogenes or tumor suppressors. Future studies will help to further elucidate the multimodal roles of circRNAs in oncogenesis.

Data available on request owing to privacy

All supporting data of this work, which are not available in public because of the ethical restrictions are available from the corresponding author upon request.

Consent for publication

All authors are consent to publication.

CONCLUSIONS

In summary, we have characterized a novel circular RNA, circ-DNAH1, which acts as a tumor suppressor in OS development and serves as an independent prognostic factor for OS patients. Targeting circ-DNAH1/miR-663a axis could be a novel strategy to develop new regimen to treat OS.

AUTHOR CONTRIBUTIONS

Peifeng Li designed the project. Ying Zhang collected data. Shimin Mu analyzed the data and drafted the manuscript. Jitian Li did almost all the experiments and were involved in data collection and analysis. All the authors revised and corrected the manuscript.

ACKNOWLEDGMENTS

We thank the reviewers for their constructive comments.

CONFLICTS OF INTEREST

The authors declared no conflicts of interest in this work.

FUNDING

This work was supported by the Major Project of TCM research in Henan Province (2019ZYZD02 and 20-21ZYZD12), the Program of Medical and Health Guidance in Luoyang City (2101043A) and the science and technology development plan project (medical and health) in Luoyang City (2101043A).

REFERENCES

1. Ottaviani G, Jaffe N. The epidemiology of osteosarcoma. Cancer Treat Res. 2009; 152:3–13.

https://doi.org/10.1007/978-1-4419-0284-9_1
PMID:20213383

2. Smrke A, Anderson PM, Gulia A, Gennatas S, Huang PH, Jones RL. Future Directions in the Treatment of Osteosarcoma. Cells. 2021; 10:172. https://doi.org/10.3390/cells10010172 PMID:33467756

3. Luetke A, Meyers PA, Lewis I, Juergens H. Osteosarcoma treatment - where do we stand? A state of the art review. Cancer Treat Rev. 2014; 40:523–32. https://doi.org/10.1016/j.ctrv.2013.11.006 PMID:24345772

4. Clark JC, Dass CR, Choong PF. A review of clinical and molecular prognostic factors in osteosarcoma. J Cancer Res Clin Oncol. 2008; 134:281–97. https://doi.org/10.1007/s00432-007-0330-x PMID:17965883

5. Bielack SS, Kempf-Bielack B, Delling G, Exner GU, Flege S, Helmke K, Kotz R, Salzer-Kuntschik M, Werner M, Winkelmann W, Zoubek A, Jürgens H, Winkler K. Prognostic factors in high-grade osteosarcoma of the extremities or trunk: an analysis of 1,702 patients treated on neoadjuvant cooperative osteosarcoma study group protocols. J Clin Oncol. 2002; 20:776–90. https://doi.org/10.1200/JCO.2002.20.3.776 PMID:11821461

6. Kempf-Bielack B, Bielack SS, Jürgens H, Branscheid D, Berdel WE, Exner GU, Göbel U, Helmke K, Jundt G, Kabisch H, Kevric M, Klingebiel T, Kotz R, et al. Osteosarcoma relapse after combined modality therapy: an analysis of unselected patients in the Cooperative Osteosarcoma Study Group (COSS). J Clin Oncol. 2005; 23:559–68. https://doi.org/10.1200/JCO.2005.04.063 PMID:15659502

7. Kager L, Zoubek A, Pötschger U, Kastner U, Flege S, Kempf-Bielack B, Branscheid D, Kotz R, Salzer-Kuntschik M, Winkelmann W, Jundt G, Kabisch H, Reichardt P, et al, and Cooperative German-Austrian-Swiss Osteosarcoma Study Group. Primary metastatic osteosarcoma: presentation and outcome of patients treated on neoadjuvant Cooperative Osteosarcoma Study Group protocols. J Clin Oncol. 2003; 21:2011–18. https://doi.org/10.1200/JCO.2003.08.132 PMID:12743156

8. Chen X, Bahrami A, Pappo A, Easton J, Dalton J, Hedlund E, Ellison D, Shurtleff S, Wu G, Wei L, Parker M, Rusch M, Nagahawatte P, et al, and St. Jude Children's Research Hospital–Washington University Pediatric Cancer Genome Project. Recurrent somatic structural variations contribute to tumorigenesis in pediatric osteosarcoma. Cell Rep. 2014; 7:104–12. https://doi.org/10.1016/j.celrep.2014.03.003 PMID:24703847

9. Perry JA, Kiezun A, Tonzi P, Van Allen EM, Carter SL, Baca SC, Cowley GS, Bhatt AS, Rheinbay E, Pedamallu CS, Helman E, Taylor-Weiner A, McKenna A, et al. Complementary genomic approaches highlight the PI3K/mTOR pathway as a common vulnerability in osteosarcoma. Proc Natl Acad Sci USA. 2014; 111:E5564–73. https://doi.org/10.1073/pnas.1419260111 PMID:25512523

10. Kelly AD, Haibe-Kains B, Janeway KA, Hill KE, Howe E, Goldsmith J, Kurek K, Perez-Atayde AR, Francoeur N, Fan JB, April C, Schneider H, Gebhardt MC, et al. MicroRNA paraffin-based studies in osteosarcoma reveal reproducible independent prognostic profiles at 14q32. Genome Med. 2013; 5:2. https://doi.org/10.1186/gm406 PMID:23339462

11. Sarver AL, Thayanithy V, Scott MC, Cleton-Jansen AM, Hogendoorn PC, Modiano JF, Subramanian S. MicroRNAs at the human 14q32 locus have prognostic significance in osteosarcoma. Orphanet J Rare Dis. 2013; 8:7. https://doi.org/10.1186/1750-1172-8-7 PMID:23311495

12. Memczak S, Jens M, Elefsinioti A, Torti F, Krueger J, Rybak A, Maier L, Mackowiak SD, Gregersen LH, Munschauer M, Loewer A, Ziebold U, Landthaler M, et al. Circular RNAs are a large class of animal RNAs with regulatory potency. Nature. 2013; 495:333–38. https://doi.org/10.1038/nature11928 PMID:23446348

13. Hansen TB, Jensen TI, Clausen BH, Bramsen JB, Finsen B, Damgaard CK, Kjems J. Natural RNA circles function as efficient microRNA sponges. Nature. 2013; 495:384–88. https://doi.org/10.1038/nature11993 PMID:23446346

14. Hansen TB, Wiklund ED, Bramsen JB, Villadsen SB, Statham AL, Clark SJ, Kjems J. miRNA-dependent gene silencing involving Ago2-mediated cleavage of a circular antisense RNA. EMBO J. 2011; 30:4414–22. https://doi.org/10.1038/emboj.2011.359 PMID:21964070

15. Kristensen LS, Hansen TB, Venø MT, Kjems J. Circular RNAs in cancer: opportunities and challenges in the field. Oncogene. 2018; 37:555–65. https://doi.org/10.1038/onc.2017.361 PMID:28991235

16. Hansen TB, Kjems J, Damgaard CK. Circular RNA and miR-7 in cancer. Cancer Res. 2013; 73:5609–12. https://doi.org/10.1158/0008-5472.CAN-13-1568 PMID:24014594

17. Zhang H, Wang G, Ding C, Liu P, Wang R, Ding W, Tong D, Wu D, Li C, Wei Q, Zhang X, Li D, Liu P, et al.

Increased circular RNA UBAP2 acts as a sponge of miR-143 to promote osteosarcoma progression. Oncotarget. 2017; 8:61687–97. https://doi.org/10.18632/oncotarget.18671 PMID:28977896

18. Jin H, Jin X, Zhang H, Wang W. Circular RNA hsa-circ-0016347 promotes proliferation, invasion and metastasis of osteosarcoma cells. Oncotarget. 2017; 8:25571–81. https://doi.org/10.18632/oncotarget.16104 PMID:28424426

19. Xu B, Yang T, Wang Z, Zhang Y, Liu S, Shen M. CircRNA CDR1as/miR-7 signals promote tumor growth of osteosarcoma with a potential therapeutic a nd diagnostic value. Cancer Manag Res. 2018; 10:4871–80. https://doi.org/10.2147/CMAR.S178213 PMID:30425578

20. Liu W, Zhang J, Zou C, Xie X, Wang Y, Wang B, Zhao Z, Tu J, Wang X, Li H, Shen J, Yin J. Microarray Expression Profile and Functional Analysis of Circular RNAs in Osteosarcoma. Cell Physiol Biochem. 2017; 43:969–85. https://doi.org/10.1159/000481650 PMID:28957794

21. Ma Q, Zhang Y, Liang H, Zhang F, Liu F, Chen S, Hu Y, Jiang L, Hao Y, Li M, Liu Y. EMP3, which is regulated by miR-663a, suppresses gallbladder cancer progression via interference with the MAPK/ERK pathway. Cancer Lett. 2018; 430:97–108. https://doi.org/10.1016/j.canlet.2018.05.022 PMID:29778567

22. Cheung KJ, Gabrielson E, Werb Z, Ewald AJ. Collective invasion in breast cancer requires a conserved basal epithelial program. Cell. 2013; 155:1639–51. https://doi.org/10.1016/j.cell.2013.11.029 PMID:24332913

23. Beavon IR. The E-cadherin-catenin complex in tumour metastasis: structure, function and regulation. Eur J Cancer. 2000; 36:1607–20. https://doi.org/10.1016/s0959-8049(00)00158-1 PMID:10959047

24. Arndt CA, Rose PS, Folpe AL, Laack NN. Common musculoskeletal tumors of childhood and adolescence. Mayo Clin Proc. 2012; 87:475–87. https://doi.org/10.1016/j.mayocp.2012.01.015 PMID:22560526

25. Whelan JS, Bielack SS, Marina N, Smeland S, Jovic G, Hook JM, Krailo M, Anninga J, Butterfass-Bahloul T, Böhling T, Calaminus G, Capra M, Deffenbaugh C, et al, and EURAMOS collaborators. EURAMOS-1, an international randomised study for osteosarcoma: results from pre-randomisation treatment. Ann Oncol. 2015; 26:407–14. https://doi.org/10.1093/annonc/mdu526 PMID:25421877

26. Moriarity BS, Otto GM, Rahrmann EP, Rathe SK, Wolf NK, Weg MT, Manlove LA, LaRue RS, Temiz NA, Molyneux SD, Choi K, Holly KJ, Sarver AL, et al. A Sleeping Beauty forward genetic screen identifies new genes and pathways driving osteosarcoma development and metastasis. Nat Genet. 2015; 47:615–24. https://doi.org/10.1038/ng.3293 PMID:25961939

27. Mirabello L, Koster R, Moriarity BS, Spector LG, Meltzer PS, Gary J, Machiela MJ, Pankratz N, Panagiotou OA, Largaespada D, Wang Z, Gastier-Foster JM, Gorlick R, et al. A Genome-Wide Scan Identifies Variants in NFIB Associated with Metastasis in Patients with Osteosarcoma. Cancer Discov. 2015; 5:920–31. https://doi.org/10.1158/2159-8290.CD-15-0125 PMID:26084801

28. Huang C, Sun Y, Ma S, Vadamootoo AS, Wang L, Jin C. Identification of circulating miR-663a as a potential biomarker for diagnosing osteosarcoma. Pathol Res Pract. 2019; 215:152411. https://doi.org/10.1016/j.prp.2019.04.003 PMID:30987831

29. Wu P, Mo Y, Peng M, Tang T, Zhong Y, Deng X, Xiong F, Guo C, Wu X, Li Y, Li X, Li G, Zeng Z, Xiong W. Emerging role of tumor-related functional peptides encoded by lncRNA and circRNA. Mol Cancer. 2020; 19:22. https://doi.org/10.1186/s12943-020-1147-3 PMID:32019587

30. Zheng J, Liu X, Xue Y, Gong W, Ma J, Xi Z, Que Z, Liu Y. TTBK2 circular RNA promotes glioma malignancy by regulating miR-217/HNF1β/Derlin-1 pathway. J Hematol Oncol. 2017; 10:52. https://doi.org/10.1186/s13045-017-0422-2 PMID:28219405

31. Hanniford D, Ulloa-Morales A, Karz A, Berzoti-Coelho MG, Moubarak RS, Sánchez-Sendra B, Kloetgen A, Davalos V, Imig J, Wu P, Vasudevaraja V, Argibay D, Lilja K, et al. Epigenetic Silencing of CDR1as Drives IGF2BP3-Mediated Melanoma Invasion and Metastasis. Cancer Cell. 2020; 37:55–70.e15. https://doi.org/10.1016/j.ccell.2019.12.007 PMID:31935372

32. Li X, Zheng Y, Zheng Y, Huang Y, Zhang Y, Jia L, Li W. Circular RNA CDR1as regulates osteoblastic differentiation of periodontal ligament stem cells via the miR-7/GDF5/SMAD and p38 MAPK signaling pathway. Stem Cell Res Ther. 2018; 9:232. https://doi.org/10.1186/s13287-018-0976-0 PMID:30170617

SUPPLEMENTARY MATERIALS

Supplementary Figures

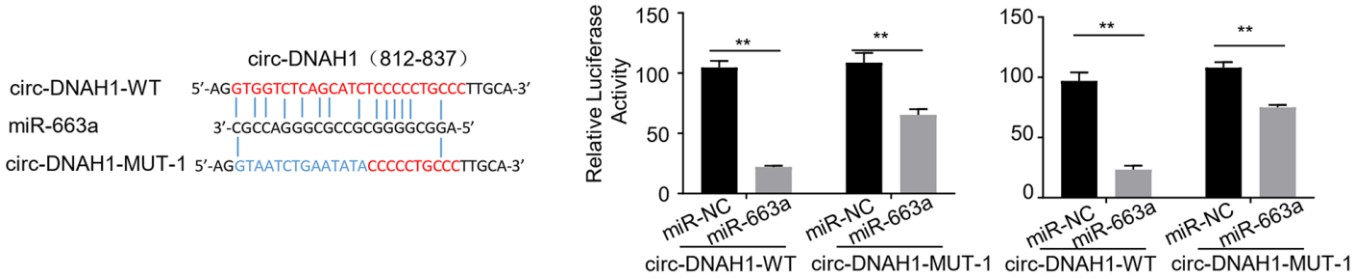

Supplementary Figure 1. Luciferase reporter analysis of MG63 and U2OS cells transfected with wild-type circ- DNAH1 WT and circ-DNAH1-MUT1. Circ-DNAH1-MUT1 partially reversed the inhibitory effect of circ-DNAH1 on miR-663a target gene expression.

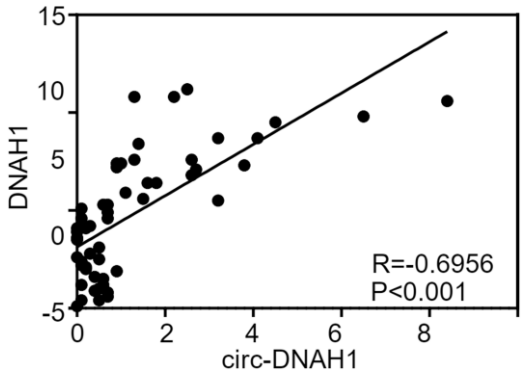

Supplementary Figure 2. Correlation between circ-DNAH1 and linear DNAH1 mRNA expression.

Supplementary Table

Supplementary Table 1. Sequences of qRT-PCR primers and siRNAs.

Primers of qRT-PCR	circ-DNAH1 Forward (5'-3')	GGCTATGGAGTCCTTGTCCC
	circ-DNAH1 Reverse (5'-3')	CCGAAGCTCCCTTCAAGACC
	GAPDH Forward (5'-3')	GGAGCGAGATCCCTCCAAAAT
	GAPDH Reverse (5'-3')	GGCTGTTGTCATACTTCTCATGG
	miR-663a Forward (5'-3')	AGGCGGGGCGCCGCGG
	miR-663a Reverse (5'-3')	GTGCAGGGTCCGAGGT
	U6 Forward (5'-3')	CTCGCTTCGGCAGCACA
	U6 Forward (5'-3')	AACGCTTCACGAATTTGCGT
siRNAs	circ-DNAH1	TTGACAATGAGGACTTTGACTGC
	NC	TTCTCCGAACGTGTCACGT